

Velocity-metallicity correlation for high- z DLA galaxies: Evidence for a mass-metallicity relation ?[★]

C. Ledoux¹, P. Petitjean^{2,3}, J. P. U. Fynbo⁴, P. Møller⁵, and R. Srianand⁶

¹ European Southern Observatory, Alonso de Córdova 3107, Casilla 19001, Vitacura, Santiago 19, Chile
e-mail: cledoux@eso.org

² Institut d'Astrophysique de Paris – UMR 7095 CNRS & Université Pierre et Marie Curie, 98bis Boulevard Arago, 75014 Paris, France
e-mail: petitjean@iap.fr

³ LERMA, Observatoire de Paris, 61 Avenue de l'Observatoire, 75014 Paris, France

⁴ Dark Cosmology Centre, Niels Bohr Institute, University of Copenhagen, Juliane Maries Vej 30, 2100 Copenhagen Ø, Denmark
e-mail: jfynbo@astro.ku.dk

⁵ European Southern Observatory, Karl-Schwarzschild-Straße 2, 85748 Garching bei München, Germany
e-mail: pmoller@eso.org

⁶ Inter-University Centre for Astronomy and Astrophysics, Post Bag 4, Ganesh Khind, Pune 411 007, India
e-mail: anand@iucaa.ernet.in

Received date / Accepted date

Abstract. We used our database of VLT-UVES quasar spectra to build up a sample of 70 Damped Lyman- α (DLA) or strong sub-DLA systems with total neutral hydrogen column densities of $\log N(\text{H I}) \geq 20$ and redshifts in the range $1.7 < z_{\text{abs}} < 4.3$. For each of the systems, we measured in an homogeneous manner the metallicities relative to Solar, $[\text{X}/\text{H}]$ (with $\text{X} = \text{Zn}$, or S or Si), and the velocity widths of low-ionization line profiles, ΔV . We provide for the first time evidence for a correlation between DLA metallicity and line profile velocity width, which is detected at the 6.1σ significance level. This confirms the trend previously observed in a much smaller sample by Wolfe & Prochaska (1998). The best-fit linear relation is $[\text{X}/\text{H}] = 1.55(\pm 0.12) \log \Delta V - 4.33(\pm 0.23)$ with ΔV expressed in km s^{-1} . The slope of the DLA velocity-metallicity relation is the same within uncertainties between the higher ($z_{\text{abs}} > 2.43$) and the lower ($z_{\text{abs}} \leq 2.43$) redshift halves of our sample. However, the two populations of systems are statistically different. There is a strong redshift evolution in the sense that the mean metallicity and mean velocity width increase with decreasing redshift. We argue that the existence of a DLA velocity-metallicity correlation, over more than a factor of 100 spread in metallicity, is probably the consequence of an underlying mass-metallicity relation for the galaxies responsible for DLA absorption lines. Assuming a simple linear scaling of the galaxy luminosity with the mass of the dark-matter halo, we find that the slope of the DLA velocity-metallicity relation is consistent with that of the luminosity-metallicity relation derived for local galaxies. If the galaxy dynamical mass is indeed the dominant factor setting up the observed DLA velocity-metallicity correlation, then the DLA systems exhibiting the lowest metallicities among the DLA population should, on average, be associated with galaxies of lower masses (e.g., gas-rich dwarf galaxies). In turn, these galaxies should have the lowest luminosities among the DLA galaxy population. This could explain the difficulties of detecting high-redshift DLA galaxies in emission.

Key words. galaxies: halos – galaxies: high-redshift – galaxies: ISM – quasars: absorption lines – cosmology: observations

1. Introduction

Over the past decade, significant progress in our understanding of early galaxy evolution has been made with large samples of high-redshift galaxies drawn from deep multi-band imaging (Steidel et al. 2003, and references therein). However, even

before the first surveys for Lyman-Break Galaxies (LBGs) had begun, samples of DLA absorbers observed on the lines-of-sight to distant quasars had been constructed (Wolfe et al. 1986, 1995). These absorbers were thought at the time to be the best carriers of information on the population of high-redshift galaxies, but, despite many attempts to identify the galaxies responsible for DLA absorption lines [hereafter called DLA galaxies], only very few could be detected in emission (see, e.g., Møller & Warren 1993; Djorgovski et al. 1996; Leibundgut & Robertson 1999; Fynbo et al. 1999; Møller et al.

[★] Based on data gathered at the European Southern Observatory (ESO) using the Ultraviolet and Visible Echelle Spectrograph (UVES) installed at the Very Large Telescope (VLT), Unit-2, Kueyen, on Cerro Paranal in Chile.

2002, 2004; Christensen et al. 2004; Weatherley et al. 2005). However, there is little doubt that DLA systems arise from the densest regions of the Universe and are closely associated with galaxies. It is therefore crucial to establish the connection between the absorption-selected DLA systems and emission-selected galaxies. In addition, the detailed information that becomes available only through the combination of morphology, colour and luminosity, with QSO absorption-line spectroscopy, makes these galaxy/absorber associations unique laboratories to study the physical processes at work during galaxy formation (see Pei et al. 1999).

Progress in this field has been slow. Firstly, a huge amount of work is needed to derive important parameters in DLA systems such as gas kinematics, metallicity, or dust and molecular fractions (see, e.g., Pettini et al. 1997; Prochaska & Wolfe 1997, 1998, 1999; Prochaska et al. 2001; Ledoux et al. 1998, 2003). Secondly, as mentioned above, the known high-redshift DLA systems have proved to be very difficult to detect in emission. This has caused some confusion and for a while suggestions were put forward that DLA absorbers may not be related to high-redshift galaxies at all. Mo et al. (1998) and Haehnelt et al. (1998b, 2000) resolved this issue showing that the difficulty of detecting high-redshift DLA systems in emission is an unavoidable consequence of the absorption cross-section selection which tends to reveal faint galaxies because they have an integrated cross-section larger than that of bright galaxies (see also Fynbo et al. 1999).

Recently, Møller et al. (2004) tentatively suggested that, if a galaxy luminosity-metallicity relation similar to that observed at $0 \lesssim z \lesssim 1$ (e.g., Garnett 2002; Kobulnicky et al. 2003; Lamareille et al. 2004; Tremonti et al. 2004) was already in place at high redshifts, then it would be possible to significantly increase the DLA galaxy detection probability by carefully selecting DLA systems with the highest metallicities. In fact, the few DLA galaxies that have to date been identified in emission do give support to the conjecture that a luminosity-metallicity relation was already in place at $z \approx 2 - 3$, although the result is only marginally statistically significant (Møller et al. 2004, see also Christensen et al., in prep.). This is in line with the near-Solar or even super-Solar metallicities derived for bright Lyman-break or bright K-band selected galaxies at similar redshifts (Shapley et al. 2004; de Mello et al. 2004). A mass-metallicity relation has recently been put into evidence for UV-selected star-forming galaxies at $z \sim 2.3$ by Erb et al. (2006).

In this paper, we provide for the first time evidence for the existence of a velocity-metallicity correlation for high-redshift DLA galaxies that could be the consequence of an underlying mass-metallicity relation for the galaxies responsible for DLA absorption lines. From the observation of a sample of 17 DLA systems at $z_{\text{abs}} < 3$, Wolfe & Prochaska (1998) previously showed that the DLA systems exhibiting the largest line profile velocity widths span a narrow range of high metallicities. However, these authors also suggested that systems with small velocity widths span a wide range of metallicities. Recently, Péroux et al. (2003) found a hint of an increase of the mean DLA metallicity with increasing velocity width, but the statistical significance of their result is low. In this paper, we

use our database of VLT-UVES quasar spectra to build up a sample of 70 DLA or strong sub-DLA systems with total neutral hydrogen column densities of $\log N(\text{H I}) \gtrsim 20$ and redshifts in the range $1.7 < z_{\text{abs}} < 4.3$. We present new, homogeneous measurements of DLA metallicities and line profile velocity widths in Sect. 2 and the observed velocity-metallicity relation in Sect. 3. We discuss in Sect. 4 the use of the DLA gas kinematics as a proxy for the mass of DLA galaxies and the possibility of the existence of a mass-metallicity relation for high- z DLA galaxies. We conclude in Sect. 5.

2. UVES DLA sample

2.1. Metallicity measurements

Most of the systems in our sample were selected from the follow-up of the Large Bright QSO Survey (LBQS; Wolfe et al. 1995) and observed at the ESO VLT with UVES between 2000 and 2004 in the course of a systematic search for molecular hydrogen at $z_{\text{abs}} > 1.8$ (Petitjean et al. 2000; Ledoux et al. 2003). Our total sample comprises 57 DLA systems ($\log N(\text{H I}) \geq 20.3$) and 13 strong sub-DLA systems with total neutral hydrogen column densities in the range $20.0 \lesssim \log N(\text{H I}) < 20.3$. This is only slightly lower than the classical definition for DLA systems to ensure that these absorbers are mostly neutral and share the same physical nature as classical DLA systems (see Viegas 1995).

We have carefully measured or remeasured total neutral hydrogen column densities, $\log N(\text{H I})$, and average DLA metallicities for all the systems in our sample. Results are summarized in Table 1. The absorption line analysis was performed in an homogeneous manner using standard Voigt-profile fitting techniques adopting the oscillator strengths compiled by Morton (2003). For the damping coefficients, we also adopted here the compilation by Morton (2003), which results in some cases in a slight increase of $\log N(\text{H I})$ values compared to Ledoux et al. (2003). Total metal column densities were derived as the sum of the column densities measured in individual components of the line profiles. Average gaseous metallicities relative to Solar, $[X/\text{H}] \equiv \log[N(\text{X})/N(\text{H})] - \log[N(\text{X})/N(\text{H})]_{\odot}$, were calculated using Solar abundances listed in Morton (2003), which are based on meteoritic data from Grevesse & Sauval (2002). To avoid problems related to possible depletion onto dust grains, metallicities given in Table 1 were computed for elements that are known to deplete very little in the ISM of the Galaxy. The reference element was taken to be $\text{X}=\text{Zn}$ when Zn II is detected, or else either S or Si was used (see Ledoux et al. 2003, for a discussion).

A noticeable property of this large dataset is that it samples well both ends of the DLA metallicity distribution, from $[X/\text{H}] \approx -2.6$ up to about half of Solar (see Table 1).

2.2. Low-ionization line kinematics

For each of the systems, we also determined the velocity widths of metal absorption line profiles. Low-ionization transition lines that are not strongly saturated were selected to trace the kinematics induced predominantly by gravity. For

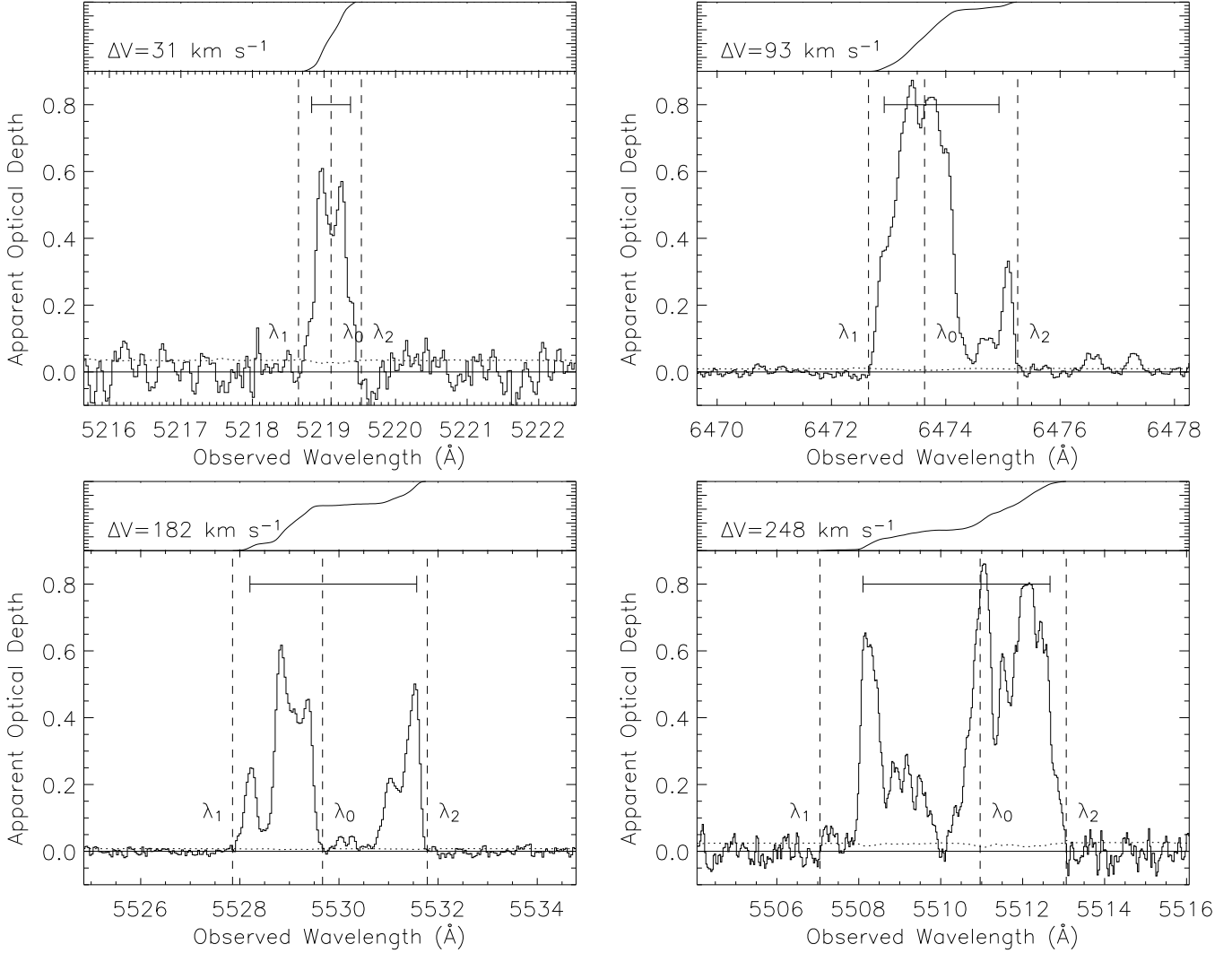


Fig. 1. Measurements of the velocity width of low-ionization line profiles, ΔV . The different panels show the apparent optical depth in the selected transition line for a given system: Si II $\lambda 1526$ at $z_{\text{abs}} = 2.418$ toward Q 0112–306 (upper left), Fe II $\lambda 1608$ at $z_{\text{abs}} = 3.025$ toward Q 0347–383 (upper right), Si II $\lambda 1526$ at $z_{\text{abs}} = 2.622$ toward Q 0405–443 (lower left), and Fe II $\lambda 1608$ at $z_{\text{abs}} = 2.426$ toward Q 2348–011 (lower right). The top part of each panel shows the integration of the apparent optical depth starting at wavelength λ_1 . The horizontal bar below that corresponds to the measurement of ΔV when 5% of the total apparent optical depth is avoided at both edges of the profile.

high-ionization lines, the velocity widths could be dominated by peculiar ejection of hot gas. We measured the line profile velocity widths following Prochaska & Wolfe (1997; see also Haehnelt et al. 1998b). We used the criterion that the residual intensity I of the strongest absorption feature in the selected line profile must satisfy $0.1 < I/I_c < 0.6$, where I_c is the intensity level of the adjacent continuum. This criterion selects transitions that are neither strongly saturated (in which case the optical depth cannot be derived and the velocity width could be overestimated), nor too weak (in which case the velocity width could be underestimated because part of the gas would be undetected). For the few systems for which none of the observed lines satisfies the above criterion, we used the mean value of the velocity widths calculated from (i) a line slightly more saturated, and (ii) a line slightly weaker, than what the criterion specifies (see Table 1). From visual inspection of the strongest

low-ionization line profiles of a given system, we established the velocity range over which the previously selected line profile should be integrated (this corresponds to the interval $[\lambda_1; \lambda_2]$ in Fig. 1).

In order to ease comparison with previous works (e.g., Prochaska & Wolfe 1997), we then calculated the line profile velocity width, ΔV , as $c[\lambda(95\%) - \lambda(5\%)]/\lambda_0$, where $\lambda(5\%)$ and $\lambda(95\%)$ are the wavelengths corresponding to, respectively, the five per cent and 95 per cent percentiles of the apparent optical depth distribution, and λ_0 is the first moment of this distribution (see Fig. 1). Note that all our spectra have a typical signal-to-noise ratio larger than 30. Excluding the extended wings of the line profiles avoids taking into account satellite components that are not strictly related to the bulk of the systems.

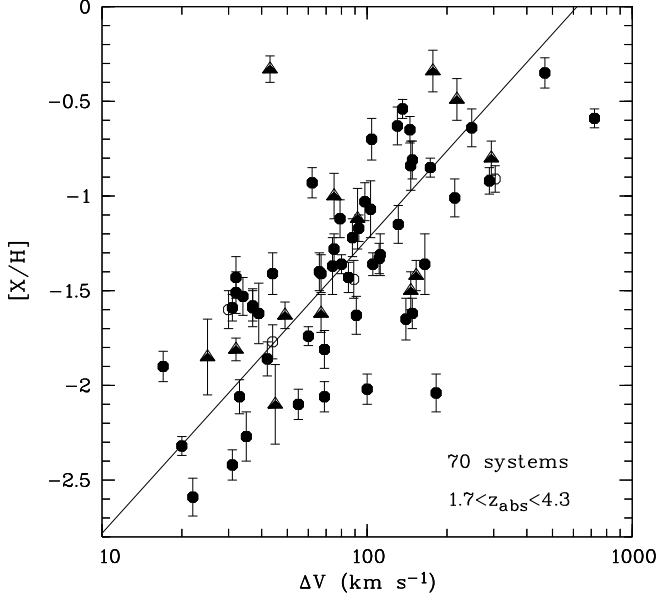


Fig. 2. Average metallicity of each of the 70 DLA or strong sub-DLA systems in our sample, $[X/H]$, vs. the velocity width of their low-ionization line profiles, ΔV , displayed on a logarithmic scale. A positive correlation between the two quantities is detected at the 6.1σ significance level using a Kendall rank correlation test. The linear least-square bisector fit is shown as a solid line. Sub-DLA systems, with total neutral hydrogen column densities $20 \lesssim \log N(\text{H I}) < 20.3$, are indicated by filled triangles. There are a few DLA systems with $c|z_{\text{em}} - z_{\text{abs}}|/(1 + z_{\text{abs}}) \leq 5000 \text{ km s}^{-1}$. For the sake of completeness, they are shown here as empty circles but they were not considered in the analysis.

3. The velocity-metallicity relation

3.1. Detected correlation

In Fig. 2, we plot on a logarithmic scale the average metallicity of each of the 70 DLA or strong sub-DLA systems in our sample, $[X/H]$, versus the velocity width of their low-ionization line profiles, ΔV . A positive correlation between the two quantities is detected at the 6.1σ significance level using a Kendall rank correlation test. Note that the DLA and strong sub-DLA populations are statistically indistinguishable even though the mean metallicity is slightly larger among sub-DLA systems. The Kolmogorov-Smirnov test probability that the two velocity width distributions (resp. metallicity distributions) are drawn from the same parent population is $P_{\text{KS}} = 0.91$ (resp. $P_{\text{KS}} = 0.72$) in the two-sided case. In the following, we therefore consider the DLA and strong sub-DLA systems in our sample altogether.

The typical measurement uncertainties in velocity width ($\pm 0.02 \text{ dex}$) and metallicity ($\pm 0.10 \text{ dex}$) are small compared to the intrinsic scatter of the data points (see Fig. 2). We thus fitted the data using the linear least-square bisector method (Isobe et al. 1990). For the correlation fits, we did not include the DLA systems with $c|z_{\text{em}} - z_{\text{abs}}|/(1 + z_{\text{abs}}) \leq 5000 \text{ km s}^{-1}$, where z_{em} is the QSO emission redshift. However, these

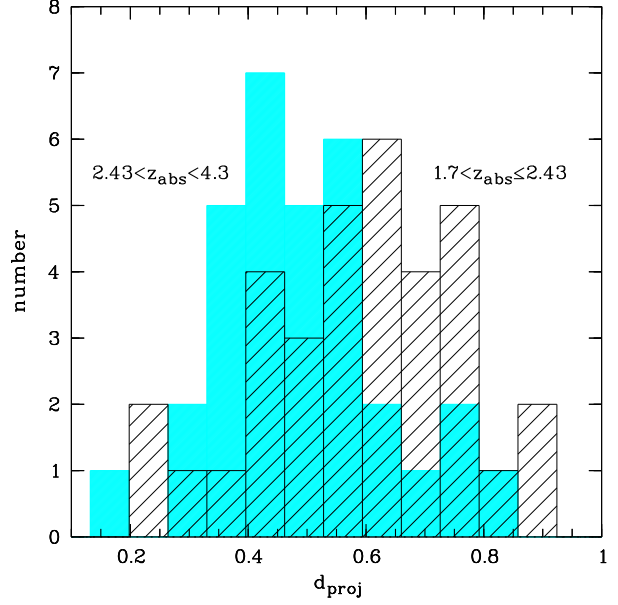


Fig. 3. Histogram of the projected position, d_{proj} , of each system along the best-fit correlation relation plotted as a solid line in Fig. 2, with $d_{\text{proj}} = 0$ (resp. $d_{\text{proj}} = 1$) at the intersection of this line with the horizontal line corresponding to $[X/H] = -3$ (resp. $[X/H] = 0$). The shaded (resp. hashed) histogram represents the higher (resp. lower) redshift half of the sample.

$z_{\text{abs}} \approx z_{\text{em}}$ systems are not associated with the central engine of the quasar, nor ejected by the quasar, but rather associated with dense gas in its surroundings (e.g., Petitjean et al. 1994; Srianand & Petitjean 2000). It can be seen in Fig. 2 that their inclusion would not affect the observed correlations and that their metallicities and line profile velocity widths are representative of those of the overall DLA population.

The best-fit linear relation is:

$$[X/H] = 1.55(\pm 0.12) \log \Delta V - 4.33(\pm 0.23) \quad (1)$$

with ΔV expressed in km s^{-1} .

The observed high-redshift velocity-metallicity correlation presented here is consistent with the results of Nestor et al. (2003) (see also Turnshek et al. 2005). Using the Sloan Digital Sky Survey (SDSS), these authors found that for strong low-ionization Mg II absorbers at $1 \lesssim z_{\text{abs}} \lesssim 2$ the Mg II $\lambda 2796$ equivalent width, or equivalently the absorption line velocity spread, is correlated with the metallicity. In addition, they showed that, within the large equivalent width regime, the average metallicity is larger at lower redshift.

3.2. Redshift evolution

The median redshift of our sample is $z_{\text{med}} = 2.43$. It can be shown that the two sub-samples of systems with, respectively, $z_{\text{abs}} > 2.43$ and $z_{\text{abs}} \leq 2.43$ differ significantly. The median DLA metallicity and median DLA velocity width increase with decreasing redshift: $[X/H] = -1.59$ and $\Delta V = 69 \text{ km s}^{-1}$, respectively, $[X/H] = -1.15$ and $\Delta V = 92 \text{ km s}^{-1}$, in the higher, respectively, the lower redshift half of the sample. This resem-

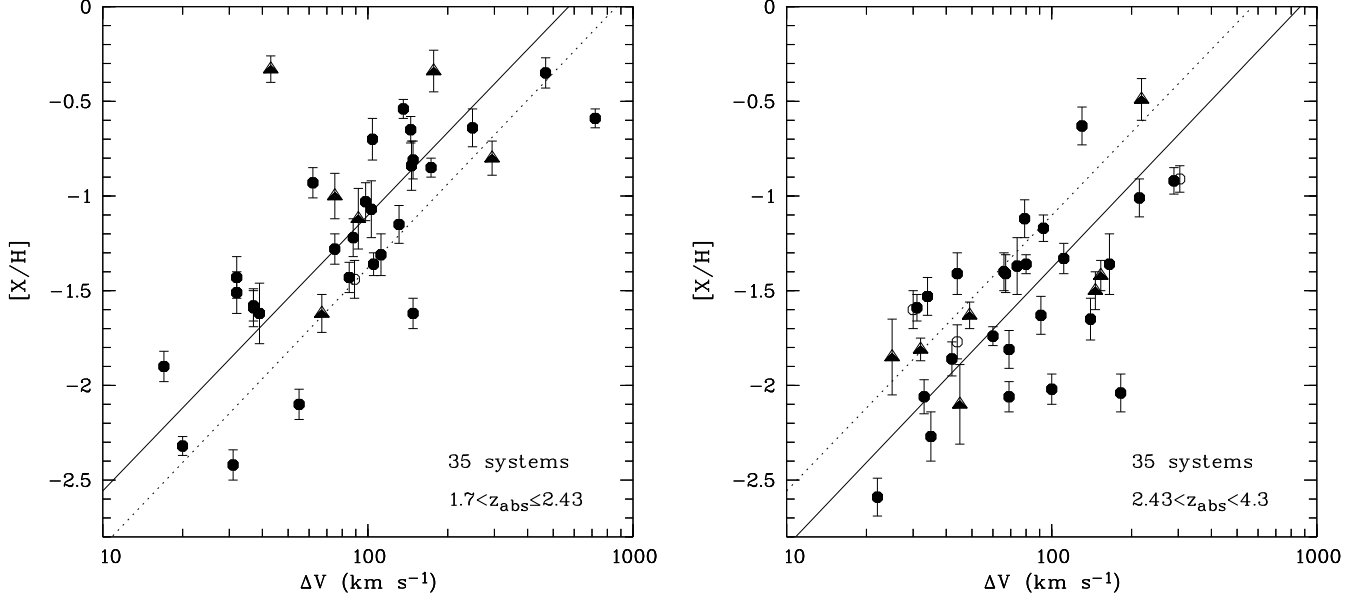


Fig. 4. Same as Fig. 2 but for the sub-sample of systems with $1.7 < z_{\text{abs}} \leq 2.43$ (left hand-side panel) or the sub-sample of systems with $2.43 < z_{\text{abs}} < 4.3$ (right hand-side panel). Positive correlations between the two quantities are detected in both the lower and the higher redshift sub-samples with significance levels of 4.6σ and 3.9σ , respectively. Linear least-square bisector fits to each sub-sample are shown as solid lines in the corresponding panels; the dotted lines are the fits to the other sub-sample. There are a few DLA systems with $c|z_{\text{em}} - z_{\text{abs}}|/(1 + z_{\text{abs}}) \leq 5000 \text{ km s}^{-1}$ in our sample. For the sake of completeness, they are shown here as empty circles but they were not considered in the analysis.

bles the point by Wolfe & Prochaska (1998) that the kinematics and metallicities of the $z_{\text{abs}} > 3$ and $z_{\text{abs}} < 3$ DLA samples could show significant differences.

To investigate this behaviour further, we have calculated for each system in our sample the projected position, d_{proj} , along the best-fit correlation relation ($[X/H]$ vs. ΔV) derived in Subsect. 3.1 and drawn as a solid line in Fig. 2. We plot in Fig. 3 the histograms of d_{proj} for the two redshift sub-samples. It is apparent that the two histograms differ in the sense that d_{proj} is larger at lower redshift. This is expected as d_{proj} increases with increasing velocity width and increasing metallicity. A Kolmogorov-Smirnov test confirms this: the two populations have only 1% chance to be drawn from the same parent population. This difference is also apparent in Fig. 4 where we plot $[X/H]$ versus ΔV for the two redshift sub-samples separately.

Considering the two redshift sub-samples separately, the best-fit linear relations are:

$$[X/H] = 1.45(\pm 0.17) \log \Delta V - 4.01(\pm 0.33) \quad (2)$$

for $1.7 < z_{\text{abs}} \leq 2.43$, and:

$$[X/H] = 1.47(\pm 0.17) \log \Delta V - 4.32(\pm 0.32) \quad (3)$$

for $2.43 < z_{\text{abs}} < 4.3$, with ΔV expressed in km s^{-1} .

The significance levels of the correlations in the lower, respectively, the higher redshift half of the sample are 4.6σ and 3.9σ , respectively (see Fig. 4). In addition, the Pearson correlation coefficients are $r = 0.72$ and 0.63 , respectively, showing that even in the high-redshift sub-sample a linear relation is a fairly good description of the data. It is very interesting to note that the correlation relations do not change significantly with

redshift although there is a statistically significant increase in both $[X/H]$ and ΔV with decreasing redshift. This is discussed in Sect. 4.

3.3. Observational scatter

Scatter in the data points is expected due to random impact parameters through the absorbing galaxies and, indeed, the scatter observed in Fig. 2 is much larger than the metallicity measurement uncertainties. Negative radial gradients in metallicity like those observed in the discs of large nearby spirals could also contribute to the scatter of the data points. This effect is probably not very important however. For instance, Chen et al. (2005) derived from a sample of six $z < 0.65$ galaxy-DLA pairs a metallicity gradient of only $-0.041 \pm 0.012 \text{ dex per kpc}$ from galactic centre to $30 h^{-1} \text{ kpc}$ radius. In addition, the magnitude of such gradients in the discs of nearby spirals has been questioned recently (Bresolin et al. 2004).

We note that there are in our sample a few systems departing from the general trend. The system at $z_{\text{abs}} = 1.973$ toward Q 0013–004 has low-ionization lines extending over up to $\sim 1100 \text{ km s}^{-1}$ in velocity space (Petitjean et al. 2002), which is much larger than for the other systems in our sample. The DLA system at $z_{\text{abs}} = 2.622$ toward Q 0405–443 has a low metallicity, $[\text{Si}/\text{H}] = -2.04$, and a comparatively large velocity width for this metallicity, $\Delta V = 182 \text{ km s}^{-1}$ (see Fig. 1, lower left-hand side panel). An inspection of these two cases indicates that the low-ionization line profiles are clumpy, being made of four and two well-separated clumps, respectively. These systems could arise in galaxy groups, tidal stream-

ing in galaxy mergers or forming galactic structures (see, e.g., Ledoux et al. 1998; Nulsen et al. 1998; Haehnelt et al. 1998b; Maller et al. 2001). The third peculiar system, the sub-DLA system at $z_{\text{abs}} = 2.287$ toward Q 2332–094, is the highest metallicity absorber in our sample with $[\text{Zn}/\text{H}] = -0.33$. It has a surprisingly small velocity width for such a high metallicity however: its profile is a blend of two sharp metal lines resulting in a velocity width of $\Delta V = 43 \text{ km s}^{-1}$. It is not unexpected to find such deviant cases in a sample that large.

4. Discussion

4.1. Kinematics as a proxy for the mass of DLA galaxies

The existence of a DLA velocity-metallicity correlation, over more than a factor of 100 spread in metallicity, can be understood as the consequence of an underlying mass-metallicity relation for the galaxies responsible for DLA absorption lines. Peculiar ejection of hot gas should indeed primarily affect the kinematics of high-ionization lines such as C IV and Si IV. Our measurements of profile velocity widths in DLA systems are based on low-ionization lines which should instead be dominated by motions on galactic scale governed or induced by gravity.

For disc galaxies, the rotation velocity is a direct measure of the galaxy’s total mass. Lines-of-sight that do not pass through the centre of the galaxy will not trace the full depth of the potential well and, therefore, will tend to show smaller velocity dispersions than the rotation velocity (see the models by Prochaska & Wolfe 1997 and Wolfe & Prochaska 1998). Hence, for random lines-of-sight through a large sample of disc galaxies, there should be a mean relationship between mass and profile velocity width, albeit with a large scatter induced by the range of impact parameters and inclination angles probed by the observations.

Infall/outflow of gas, or merging of galaxy sub-clumps, will also produce kinematically broadened line profiles with velocity widths scaling as the infall/outflow velocities, which again scale as the depth of the combined potential well of the galaxies or mergers. Simulations have shown that in that case the line profile velocity width is a good indicator of the circular velocity of the underlying dark-matter halo with $\Delta V \sim 0.6v_c$ (Nulsen et al. 1998; Haehnelt et al. 1998b; Maller et al. 2001). The scatter in this relation is about a factor of two and corresponds approximately to the width of the correlation shown in Fig. 2.

In addition, there is a positive correlation between the projected stellar mass density and the neutral hydrogen column density of DLA systems and a good correspondence in the spatial distribution of stars and DLA systems in simulations including star formation, supernova feedback and feedback by galactic winds (see Nagamine et al. 2004).

4.2. Implications and prospects

For reasons discussed above, we assume here that the dynamical mass of DLA galaxies is the dominant factor setting up the observed DLA velocity-metallicity correlation.

4.2.1. Mass-metallicity relation

The slope of the DLA velocity-metallicity relation is the same within uncertainties for the two redshift halves of our sample (see Subsect. 3.2). There is a possible increase of the intercept point of this relation with decreasing redshift (see Fig. 4) but this result is not statistically significant due to the large scatter of the data points around the mean relations (see Eqs. 2 and 3). However, the two redshift sub-samples differ in the sense that the median DLA metallicity and median DLA velocity width increase with decreasing redshift (see Subsect. 3.2 and Fig. 3). This suggests that galaxy halos of a given mass (resp. a given metallicity) are becoming more metal-rich (resp. less massive) with time.

This is consistent with the results of Savaglio et al. (2005) who proposed a redshift-dependent galaxy mass-metallicity relation from the study of $0.4 < z < 1.0$ galaxies selected from the Gemini Deep Deep Survey and the Canada-France Redshift Survey. Note also that a mass-metallicity relation has recently been put into evidence at $z \sim 2.3$ for UV-selected star-forming galaxies (Erb et al. 2006).

4.2.2. Luminosity-metallicity relation

From Cold Dark Matter (CDM) simulations, Haehnelt et al. (1998b) have shown that the velocity width of DLA systems, ΔV , can be related statistically to the circular velocity of the underlying dark-matter halo, $v_c = (GM/r)^{1/2}$, where M is the mass in a sphere overdense by a factor of 200 compared to the mean cosmic density. They found $\Delta V \sim 0.6v_c$. According to Haehnelt et al. (1998a, 2000), the luminosity function of $z \sim 3$ galaxies can be reproduced if a simple linear scaling of the luminosity with the mass of the dark-matter halo is assumed, i.e., $m_R = -7.5 \log(v_c/200 \text{ km s}^{-1}) + m_R^0$, where m_R is the galaxy apparent R -band magnitude and $m_R^0 = 26.6$ for the Λ -CDM model. Using our best-fit to the velocity-metallicity relation for $1.7 < z_{\text{abs}} \leq 2.43$ DLA systems (Eq. 2), and $z_{\text{med}} = 2.09$ for this sub-sample, we derive:

$$[\text{X}/\text{H}] = -0.19(\pm 0.02)M_R - 4.76(\pm 0.42) + 0.19(\pm 0.02)K_R \quad (4)$$

where M_R is the galaxy absolute R -band magnitude and K_R is the K -correction in the R -band. Using our best-fit to the velocity-metallicity relation for $2.43 < z_{\text{abs}} < 4.3$ DLA systems (Eq. 3) leads to a similar result.

It is striking to note that the slope of this DLA luminosity-metallicity relation is consistent with that derived by Tremonti et al. (2004) for the luminosity-metallicity relation for $z \sim 0.1$ galaxies selected from the SDSS, $[\text{O}/\text{H}] = -0.185(\pm 0.001)M_B - 3.452(\pm 0.018)$. The correction from the R -band at high redshift to the B -band at low redshift corresponds to an additional factor that corresponds to a non-positive K -correction (Kinney et al. 1996) in Eq. 4. Therefore,

the intercept points of the two luminosity-metallicity relations are different in the sense that galaxies of a given luminosity (resp. a given metallicity) are becoming more metal-rich (resp. fainter) with time.

5. Conclusions

Using a sample of 70 DLA or strong sub-DLA systems with total neutral hydrogen column densities of $\log N(\text{H I}) \gtrsim 20$ and redshifts in the range $1.7 < z_{\text{abs}} < 4.3$, we have shown that there is a correlation between metallicity ($[\text{X}/\text{H}]$) and line profile velocity width (ΔV) at the 6.1σ significance level. The best-fit linear relation is $[\text{X}/\text{H}] = 1.55(\pm 0.12) \log \Delta V - 4.33(\pm 0.23)$ with ΔV expressed in km s^{-1} . We argued that the existence of a DLA velocity-metallicity correlation, over more than a factor of 100 spread in metallicity, is probably the consequence of an underlying mass-metallicity relation for the galaxies responsible for DLA absorption lines. Assuming a simple linear scaling of the galaxy luminosity with the mass of the dark-matter halo, we found that the slope of the DLA velocity-metallicity relation is consistent with that of the luminosity-metallicity relation derived for local galaxies. If the galaxy dynamical mass is indeed the dominant factor setting up the observed DLA velocity-metallicity correlation, then the DLA systems exhibiting the lowest metallicities among the DLA population should, on average, be associated with galaxies of lower masses.

Eq. 4 implies that the more than two orders of magnitude spread in DLA metallicity could reflect a more than ten magnitudes spread in DLA galaxy luminosity. Even though low-mass galaxies, i.e., gas-rich dwarf galaxies, can undergo periods of intense star formation activity and, in this case, have high luminosities in the UV, it is a fact that, on average, they show lower star-formation rates than more massive galaxies (Brinchmann et al. 2004; see also Okoshi et al. 2004). This may well explain the difficulty of detecting high-redshift DLA galaxies in emission (e.g., Kulkarni et al. 2000, 2001). Furthermore, the non-detection of $\text{Ly}\alpha$ emission from the galaxies responsible for low-metallicity DLA systems, down to $\text{Ly}\alpha$ fluxes fainter than most of the $\text{Ly}\alpha$ emitters from the deep survey of Fynbo et al. (2003), could be a consequence of their low masses and their correspondingly, on average, low star-formation activity.

A significant fraction of DLA galaxies could be actively forming stars for some period of time, but due to their small masses the bursts of star-formation would not be powerful enough and/or would have too short life-times. $\text{Ly}\alpha$ emission would simply be too faint or would be strong for a too short spell of time to be detected by the current generation of 8-10 m class telescopes. Conversely, the existence of a DLA mass-metallicity relation can explain the recent, tentative result by Møller et al. (2004) that the few DLA systems with detected $\text{Ly}\alpha$ emission have higher than average metallicities (see also Christensen et al., in prep.). This should be confirmed by additional deep imaging of the fields of QSOs with carefully selected DLA absorbers.

The DLA velocity-metallicity correlation relation studied in this paper also needs to be investigated in the context of new high-resolution smoothed-particle hydrodynamics simulations

including the effects of feedback in a self-consistent manner (see, e.g., Nagamine et al. 2004).

Acknowledgements. We thank Sandra Savaglio for sharing results prior to publication. JPUF is supported by the Danish Natural Science Research Council (SNF). PPJ and RS gratefully acknowledge support from the Indo-French Centre for the Promotion of Advanced Research (Centre Franco-Indien pour la Promotion de la Recherche Avancée) under contract No. 3004-3. PPJ thanks ESO Vitacura for hospitality during the time part of this work has been completed.

References

- Bresolin, F., Garnett, D. R., & Kennicutt, R. C. 2004, *ApJ*, 615, 228
- Brinchmann, J., Charlot, S., White, S. D. M., et al. 2004, *MNRAS*, 351, 1151
- Chen, H.-W., Kennicutt, R. C., & Rauch, M. 2005, *ApJ*, 620, 703
- Christensen, L., Sánchez, S. F., Jahnke, K., et al. 2004, *A&A*, 417, 487
- de Mello, D. F., Daddi, E., Renzini, A., et al. 2004, *ApJ*, 608, L29
- Djorgovski, S. G., Pahre, M. A., Bechtold, J., & Elston, R. 1996, *Nature*, 382, 234
- Erb, D. K., Shapley, A. E., Pettini, M., et al. 2006, *ApJ*, in press [astro-ph/0602473]
- Fynbo, J. P. U., Ledoux, C., Møller, P., Thomsen, B., & Burud, I. 2003, *A&A*, 407, 147
- Fynbo, J. P. U., Møller, P., & Warren, S. J. 1999, *MNRAS*, 305, 849
- Garnett, D. R. 2002, *ApJ*, 581, 1019
- Grevesse, N. & Sauval, A. J. 2002, *Adv. Space Res.*, 30, 3
- Haehnelt, M. G., Natarajan, P., & Rees, M. J. 1998a, *MNRAS*, 300, 817
- Haehnelt, M. G., Steinmetz, M., & Rauch, M. 1998b, *ApJ*, 495, 647
- Haehnelt, M. G., Steinmetz, M., & Rauch, M. 2000, *ApJ*, 534, 594
- Isobe, T., Feigelson, E. D., Akritas, M. G., & Babu, G. J. 1990, *ApJ*, 364, 104
- Kinney, A. L., Calzetti, D., Bohlin, R. C., et al. 1996, *ApJ*, 467, 38
- Kobulnicky, H. A., Willmer, C. N. A., Phillips, A. C., et al. 2003, *ApJ*, 599, 1006
- Kulkarni, V. P., Hill, J. M., Schneider, G., et al. 2000, *ApJ*, 536, 36
- Kulkarni, V. P., Hill, J. M., Schneider, G., et al. 2001, *ApJ*, 551, 37
- Lamareille, F., Mouhcine, M., Contini, T., Lewis, I., & Maddox, S. 2004, *MNRAS*, 350, 396
- Ledoux, C., Petitjean, P., Bergeron, J., Wampller, E. J., & Srianand, R. 1998, *A&A*, 337, 51
- Ledoux, C., Petitjean, P., & Srianand, R. 2003, *MNRAS*, 346, 209
- Ledoux, C., Petitjean, P., & Srianand, R. 2006, *ApJ*, 640, L25
- Ledoux, C., Srianand, R., & Petitjean, P. 2002, *A&A*, 392, 781
- Leibundgut, B. & Robertson, J. G. 1999, *MNRAS*, 303, 711
- Maller, A. H., Prochaska, J. X., Somerville, R. S., & Primack, J. R. 2001, *MNRAS*, 326, 1475
- Mo, H. J., Mao, S., & White, S. D. M. 1998, *MNRAS*, 295, 319
- Molaro, P., Levshakov, S. A., D’Odorico, S., Bonifacio, P., & Centurión, M. 2001, *ApJ*, 549, 90
- Møller, P., Fynbo, J. P. U., & Fall, S. M. 2004, *A&A*, 422, L33
- Møller, P. & Warren, S. J. 1993, *A&A*, 270, 43
- Møller, P., Warren, S. J., Fall, S. M., Fynbo, J. P. U., & Jakobsen, P. 2002, *ApJ*, 574, 51
- Morton, D. C. 2003, *ApJS*, 149, 205
- Nagamine, K., Springel, V., & Hernquist, L. 2004, *MNRAS*, 348, 435
- Nestor, D. B., Rao, S. M., Turnshek, D. A., & Vanden Berk, D. 2003, *ApJ*, 595, L5
- Nulsen, P. E. J., Barcons, X., & Fabian, A. C. 1998, *MNRAS*, 301, 168

- Okoshi, K., Nagashima, M., Gouda, N., & Yoshioka, S. 2004, *ApJ*, 603, 12
- Pei, Y. C., Fall, S. M., & Hauser, M. G. 1999, *ApJ*, 522, 604
- Péroux, C., Dessauges-Zavadsky, M., D’Odorico, S., Kim, T.-S., & McMahon, R. G. 2003, *MNRAS*, 345, 480
- Petitjean, P., Rauch, M., & Carswell, R. F. 1994, *A&A*, 291, 29
- Petitjean, P., Srianand, R., & Ledoux, C. 2000, *A&A*, 364, L26
- Petitjean, P., Srianand, R., & Ledoux, C. 2002, *MNRAS*, 332, 383
- Pettini, M., Smith, L. J., King, D. L., & Hunstead, R. W. 1997, *ApJ*, 486, 665
- Prochaska, J. X., Gawiser, E., & Wolfe, A. M. 2001, *ApJ*, 552, 99
- Prochaska, J. X. & Wolfe, A. M. 1997, *ApJ*, 487, 73
- Prochaska, J. X. & Wolfe, A. M. 1998, *ApJ*, 507, 113
- Prochaska, J. X. & Wolfe, A. M. 1999, *ApJS*, 121, 369
- Savaglio, S., Glazebrook, K., Le Borgne, D., et al. 2005, *ApJ*, 635, 260
- Shapley, A. E., Erb, D. K., Pettini, M., Steidel, C. C., & Adelberger, K. L. 2004, *ApJ*, 612, 108
- Srianand, R. & Petitjean, P. 2000, *A&A*, 357, 414
- Steidel, C. C., Adelberger, K. L., Shapley, A. E., et al. 2003, *ApJ*, 592, 728
- Tremonti, C. A., Heckman, T. M., Kauffmann, G., et al. 2004, *ApJ*, 613, 898
- Turnshek, D. A., Rao, S. M., Nestor, D. B., Belfort-Mihalyi, M., & Quider, A. M. 2005, in Williams P. R., Shu C., & Ménard B., eds., *Proc. IAU Colloquium No. 199, Probing Galaxies through Quasar Absorption Lines*. [astro-ph/0506701]
- Viegas, S. M. 1995, *MNRAS*, 276, 268
- Weatherley, S. J., Warren, S. J., Møller, P., et al. 2005, *MNRAS*, 358, 985
- Wolfe, A. M., Lanzetta, K. M., Foltz, C. B., & Chaffee, F. H. 1995, *ApJ*, 454, 698
- Wolfe, A. M. & Prochaska, J. X. 1998, *ApJ*, 494, L15
- Wolfe, A. M., Turnshek, D. A., Smith, H. E., & Cohen, R. D. 1986, *ApJS*, 61, 249

Table 1. UVES DLA sample: average metallicities and velocity widths of low-ionisation line profiles *

Quasar	Other name	z_{em}	z_{abs}^1	$\log N(\text{H I})$	$[\text{X}/\text{H}]^2$	X	ΔV (km s^{-1})	Selected transition lines ³
Q 0000–263	LBQS 0000–2619	4.11	3.390	21.40 ± 0.08	-2.06 ± 0.09	Zn	33	O I λ 950
Q 0010–002	LBQS 0010–0012	2.15	2.025	20.95 ± 0.10	-1.43 ± 0.11	Zn	32	Si II λ 1808
Q 0013–004	LBQS 0013–0029	2.09	1.973	20.83 ± 0.05	-0.59 ± 0.05	Zn	720	Fe II λ 1608
Q 0058–292	LBQS 0058–2914	3.09	2.671	21.10 ± 0.10	-1.53 ± 0.10	Zn	34	Si II λ 1808
Q 0100+130	LBQS 0100+1300	2.69	2.309	21.35 ± 0.08	-1.58 ± 0.08	Zn	37	Cr II λ 2056
Q 0102–190	LBQS 0102–1902	3.04	2.370	21.00 ± 0.08	-1.90 ± 0.08	S	17	Fe II λ 2374
Q 0102–190	LBQS 0102–1902	3.04	2.926	20.00 ± 0.10	-1.50 ± 0.10	Si	146	Si II λ 1526
Q 0112–306	LBQS 0112–3041	2.99	2.418	20.50 ± 0.08	-2.42 ± 0.08	Si	31	Si II λ 1526
Q 0112–306	LBQS 0112–3041	2.99	2.702	20.30 ± 0.10	-0.49 ± 0.11	Si	218	Fe II λ 1608
Q 0112+030	LBQS 0112+0300	2.81	2.423	20.90 ± 0.10	-1.31 ± 0.11	S	112	Fe II λ 1608
Q 0135–273	CTS 1005	3.21	2.107	20.30 ± 0.15	-1.12 ± 0.16	S	82/103	Fe II λ 2260/Fe II λ 2586
Q 0135–273	CTS 1005	3.21	2.800	21.00 ± 0.10	-1.40 ± 0.10	S	65/67	S II λ 1259/Fe II λ 1608
Q 0216+080	LBQS 0216+0803	2.99	1.769	20.30 ± 0.10	-1.00 ± 0.12	Zn	75	Fe II λ 2374
Q 0216+080	LBQS 0216+0803	2.99	2.293	20.50 ± 0.10	-0.70 ± 0.11	Zn	104	Si II λ 1808
Q 0336–017	LBQS 0336–0142	3.20	3.062	21.10 ± 0.10	-1.41 ± 0.10	Si	67	Si II λ 1808
Q 0347–383	LBQS 0347–3819	3.22	3.025	20.73 ± 0.05	-1.17 ± 0.07	Zn	93	Fe II λ 1608
Q 0405–443	CTS 247	3.02	1.913	20.80 ± 0.10	-1.03 ± 0.10	Zn	98	Si II λ 1808
Q 0405–443	CTS 247	3.02	2.550	21.15 ± 0.15	-1.36 ± 0.16	Zn	165	Si II λ 1808
Q 0405–443	CTS 247	3.02	2.595	21.05 ± 0.10	-1.12 ± 0.10	Zn	79	Si II λ 1808
Q 0405–443	CTS 247	3.02	2.622	20.45 ± 0.10	-2.04 ± 0.10	Si	182	Si II λ 1526
Q 0450–131	2.25	2.067	20.50 ± 0.07	-1.62 ± 0.08	S	148	Fe II λ 1608
Q 0458–020	LBQS 0458–0203	2.29	2.040	21.70 ± 0.10	-1.22 ± 0.10	Zn	88	Cr II λ 2056
Q 0528–250	LBQS 0528–2505	2.77	2.141	20.98 ± 0.05	-1.36 ± 0.06	Zn	105	Si II λ 1808
Q 0528–250	LBQS 0528–2505	2.77	2.811	21.35 ± 0.07	-0.91 ± 0.07	Zn	304	S II λ 1253
Q 0551–366	2.32	1.962	20.70 ± 0.08	-0.35 ± 0.08	Zn	468	Si II λ 1808
Q 0841+129	2.50	1.864	21.00 ± 0.10	-1.51 ± 0.11	S	32	S II λ 1259
Q 0841+129	2.50	2.375	21.05 ± 0.10	-1.59 ± 0.10	Zn	37	Fe II λ 1125
Q 0841+129	2.50	2.476	20.80 ± 0.10	-1.60 ± 0.10	Zn	30	S II λ 1259
Q 0913+072	LBQS 0913+0715	2.78	2.618	20.35 ± 0.10	-2.59 ± 0.10	Si	22	Si II λ 1526
Q 1036–229	CTS 460	3.13	2.778	20.93 ± 0.05	-1.36 ± 0.05	S	80	Fe II λ 1081
Q 1108–077	BRI 1108–0747	3.92	3.482	19.95 ± 0.07	-1.63 ± 0.07	Si	49	Si II λ 1526
Q 1108–077	BRI 1108–0747	3.92	3.608	20.37 ± 0.07	-1.59 ± 0.07	Si	31	Fe II λ 1608
Q 1111–152	CTS 298	3.37	3.266	21.30 ± 0.05	-1.65 ± 0.11	Zn	140	Si II λ 1020
Q 1117–134	BR 1117–1329	3.96	3.350	20.95 ± 0.10	-1.41 ± 0.11	Zn	43/45	Si II λ 1808/Fe II λ 1608
Q 1157+014	1.99	1.944	21.80 ± 0.10	-1.44 ± 0.10	Zn	89	Fe II λ 2260
Q 1209+093	LBQS 1209+0919	3.30	2.584	21.40 ± 0.10	-1.01 ± 0.10	Zn	214	Si II λ 1808
Q 1210+175	LBQS 1210+1731	2.54	1.892	20.70 ± 0.08	-0.93 ± 0.08	S	62	S II λ 1253
Q 1223+178	LBQS 1223+1753	2.94	2.466	21.40 ± 0.10	-1.63 ± 0.10	Zn	91	Si II λ 1808
Q 1232+082	LBQS 1232+0815	2.57	2.338	20.90 ± 0.08	-1.43 ± 0.08	S	85	Si II λ 1808
Q 1331+170	2.08	1.776	21.15 ± 0.07	-1.28 ± 0.08	Zn	75	Fe II λ 2374
Q 1337+113	LBQS 1337+1121	2.92	2.508	20.12 ± 0.05	-1.81 ± 0.06	Si	32	Fe II λ 2344
Q 1337+113	LBQS 1337+1121	2.92	2.796	21.00 ± 0.08	-1.86 ± 0.09	Si	42	Fe II λ 1608
Q 1340–136	CTS 325	3.20	3.118	20.05 ± 0.08	-1.42 ± 0.08	S	153	Fe II λ 1608
Q 1409+095	LBQS 1409+0930	2.85	2.019	20.65 ± 0.10	-1.62 ± 0.16	Zn	39	Fe II λ 2374
Q 1409+095	LBQS 1409+0930	2.85	2.456	20.53 ± 0.08	-2.06 ± 0.08	Si	69	Si II λ 1526
Q 1441+276	PSS J 1443+2724	4.42	4.224	20.95 ± 0.10	-0.63 ± 0.10	S	130	Fe II λ 1081
Q 1444+014	LBQS 1444+0126	2.21	2.087	20.25 ± 0.07	-0.80 ± 0.09	Zn	294	Fe II λ 1608
Q 1451+123	LBQS 1451+1223	3.25	2.255	20.35 ± 0.10	-1.07 ± 0.15	Zn	103	Fe II λ 2374
Q 1451+123	LBQS 1451+1223	3.25	2.469	20.40 ± 0.10	-2.27 ± 0.13	Si	35	Fe II λ 2382
Q 1451+123	LBQS 1451+1223	3.25	3.171	20.20 ± 0.20	-2.10 ± 0.21	Si	45	Si II λ 1526
Q 2059–360	3.09	2.507	20.29 ± 0.07	-1.85 ± 0.20	S	25	Fe II λ 2344
Q 2059–360	3.09	3.083	20.98 ± 0.08	-1.77 ± 0.09	S	44	Fe II λ 1121
Q 2116–358	HES 2116–3550	2.34	1.996	20.10 ± 0.07	-0.34 ± 0.11	Zn	177	Fe II λ 1608

Table 1. continued

Quasar	Other name	z_{em}	z_{abs}^1	$\log N(\text{H I})$	$[\text{X}/\text{H}]^2$	X	ΔV (km s^{-1})	Selected transition lines ³
Q 2138–444	LBQS 2138–4427	3.17	2.383	20.60 ± 0.05	-1.15 ± 0.10	Zn	131	Fe II λ 2374
Q 2138–444	LBQS 2138–4427	3.17	2.852	20.98 ± 0.05	-1.74 ± 0.05	Zn	58/62	Si II λ 1808/Fe II λ 2374
Q 2152+137	PSS J 2155+1358	4.26	3.316	20.50 ± 0.15	-1.37 ± 0.15	Si	74	Fe II λ 1608
Q 2206–199	LBQS 2206–1958	2.56	1.921	20.67 ± 0.05	-0.54 ± 0.05	Zn	136	Si II λ 1808
Q 2206–199	LBQS 2206–1958	2.56	2.076	20.44 ± 0.05	-2.32 ± 0.05	Si	20	Si II λ 1304
Q 2230+025	LBQS 2230+0232	2.15	1.864	20.90 ± 0.10	-0.81 ± 0.10	S	148	S II λ 1253
Q 2231–002	LBQS 2231–0015	3.02	2.066	20.55 ± 0.07	-0.65 ± 0.07	S	145	S II λ 1253
Q 2243–605	HES 2243–6031	3.01	2.331	20.65 ± 0.05	-0.85 ± 0.05	Zn	173	Si II λ 1808
Q 2332–094	FIRST J 2334–0908	3.32	2.287	20.07 ± 0.07	-0.33 ± 0.07	Zn	43	Si II λ 1808
Q 2332–094	FIRST J 2334–0908	3.32	3.057	20.50 ± 0.07	-1.33 ± 0.08	S	111	Fe II λ 1608
Q 2343+125	2.51	2.431	20.40 ± 0.07	-0.92 ± 0.07	Zn	289	Fe II λ 1608
Q 2344+125	2.76	2.538	20.50 ± 0.10	-1.81 ± 0.10	Si	69	Fe II λ 1608
Q 2348–011	LBQS 2348–0108	3.01	2.426	20.50 ± 0.10	-0.64 ± 0.10	S	248	Fe II λ 1608
Q 2348–011	LBQS 2348–0108	3.01	2.615	21.30 ± 0.08	-2.02 ± 0.08	Si	95/105	Si II λ 1808/Si II λ 1526
Q 2348–147	2.94	2.279	20.63 ± 0.05	-2.10 ± 0.08	S	55	Fe II λ 2586
Q 2359–022	LBQS 2359–0216	2.81	2.095	20.65 ± 0.10	-0.84 ± 0.13	Zn	146	Fe II λ 1608
Q 2359–022	LBQS 2359–0216	2.81	2.154	20.30 ± 0.10	-1.62 ± 0.10	Si	67	Si II λ 1526

* Total neutral hydrogen column density and metallicity measurements are from this work, except for the systems at $z_{\text{abs}} = 3.390$ toward Q 0000–263 (Molaro et al. 2001), $z_{\text{abs}} = 3.025$ and 2.087 toward, respectively, Q 0347–383 and Q 1444+014 (Ledoux et al. 2003), $z_{\text{abs}} = 1.962$ toward Q 0551–366 (Ledoux et al. 2002), and $z_{\text{abs}} = 4.224$ toward Q 1441+276 (Ledoux et al. 2006).

Quoted uncertainties are 1σ standard deviations.

¹ There are a few DLA systems with $c|z_{\text{em}} - z_{\text{abs}}|/(1 + z_{\text{abs}}) < 5000 \text{ km s}^{-1}$. These systems were not considered during the correlation analyzes. However, their properties (metallicity, $N(\text{H I})$, ionisation level) do not resemble those of the associated systems. They are not associated with the central engine of the quasar, nor ejected by the quasar, but rather associated with dense gas in its surroundings (see text).

² Average gaseous metallicities relative to Solar, $[\text{X}/\text{H}] \equiv \log[N(\text{X})/N(\text{H})] - \log[N(\text{X})/N(\text{H})]_{\odot}$, calculated using Solar abundances listed in Morton (2003), which are based on meteoritic data from Grevesse & Sauval (2002). The reference element was taken to be $\text{X}=\text{Zn}$ when Zn II is detected, or else either S or Si was used.

³ Transition lines used to determine the velocity widths of low-ionisation line profiles. Whenever none of the observed lines satisfies the adopted criterion (see Sect. 2), we used the mean value of the velocity widths calculated from (i) a line slightly more saturated, and (ii) a line slightly weaker, than what the criterion specifies.